Fluorescence Generalized Polarization of Cell Membranes: A Two-Photon Scanning Microscopy Approach

Weiming Yu, Peter T. C. So, Todd French, and Enrico Gratton

Laboratory for Fluorescence Dynamics, Department of Physics, University of Illinois at Urbana-Champaign, Urbana, Illinois 61801 USA

ABSTRACT We use the lipophilic fluorescence probe Laurdan to study cell membranes. The generalized polarization (GP) of Laurdan-labeled cells contains useful information about membrane fluidity and polarity. A high GP is usually associated with low fluidity, low polarity, or high cholesterol content of the membranes, and a low GP is the opposite. We have combined the GP method and two-photon fluorescence microscopy to provide an alternative approach to study cell membranes. Using two-photon excitation in a conventional microscope offers great advantages for studying biological samples. These advantages include efficient background rejection, low photodamage, and improved depth discrimination. We performed GP measurements on mouse fibroblast cells and observed that both intensity and GP images are not spatially uniform. We tested for possible GP artifacts arising from cellular autofluorescence and lifetime quenching, using a procedure for background fluorescence subtraction and by direct lifetime measurements in the microscope. GP measured in a single cell displays a broad distribution, and the GP of 40 different cells grown on the same cover glass is also statistically distributed. The correlations between intensity and GP images were analyzed, and no monotonic dependence between the two was found. By digitally separating high and low GP values, we found that high GP values often associate with the regions of the plasma membrane and low GP values link with the nuclear membranes. Our results also show local GP variations within the plasma and nuclear membranes.

INTRODUCTION

Biological membranes define the boundaries of living cells and of their organelles. They enable cells to distinguish self from non-self. Many biological events and biochemical processes originate either directly or indirectly within the cell membranes. Since the proposal of the fluid-mosaic membrane model (Singer and Nicolson, 1972), there has been substantial progress in understanding the physical properties of membranes in regulating biological activities. In particular, membrane fluidity, and possibly the formation of lipid phase domains in relation to a variety of cellular events, has drawn the attention of many researchers (Grant, 1983; McElhaney, 1985; Maresca and Cossins, 1993; Aloia et al., 1993; Paller, 1994).

There is a large body of experimental methods used in cuvette studies that can provide biophysical information on molecular processes in membranes. Some of the methods are difficult or impossible to apply in the microscope setup. Only recently, technical advances in fluorescence microscopy have allowed a quantitative spectroscopic approach at the microscopic level. Fluorescence spectroscopy is one of the most promising methods. However, to extract quantitative information about processes at a mo-

lecular level, one must use sophisticated measurement protocols. Methods such as fluorescence photobleaching recovery and single-particle tracking give quantitative information about diffusion of membrane components at a microscopic level (Gordon et al., 1995; Zhang et al., 1993). However, there are other biophysical properties of membrane systems that one can use to obtain similar or complementary information about membrane function and dynamics on the entire cell. Here we propose using a well-established measurement protocol of membrane fluidity and dynamics that can be easily implemented in the microscope in conjunction with two-photon excitation. By extending methods that were implemented for cuvette studies to the microscope, we can address new kinds of problems related to the morphological heterogeneity of the measured parameters. We were motivated to implement known biophysical methods in the microscope by several current problems in cell biophysics, all of them centered around membrane heterogeneity. There is speculation about the functional role of membrane fluidity domains, but a clear demonstration of their existence and of their functional role is still lacking.

Various spectroscopic and microscopic methods are used in the studies of membrane structures, dynamics, and functions (Lentz, 1988; Sankaram et al., 1994; Wang and Hollinsworth, 1995; Gicquaud and Wong, 1994; Blumenthal et al., 1995; Wang et al., 1993). The spectroscopic and microscopic methods complement each other. Spectroscopic methods provide high-precision average behavior of the measured quantities. The microscopic methods, on the other hand, provide spatial information that is essential for identifying biological processes. Fluorescence polarization is commonly used as a spectroscopic method for measuring

membrane lipid fluidity and order (Jajoo et al., 1994; Serafini et al., 1993). Its complementary microscopic method has also been used in membrane studies (Florine-Casteel, 1990; Suzuki et al., 1995) but is less common for technical reasons. A lipid membrane phase transition can be followed by steady-state fluorescence polarization using 1,6-diphenyl-1,3,5-hexatriene as a probe. However, for a membrane containing mixed phase states the characteristic signal from the different phase components cannot be resolved with steady-state polarization. Instead, time-resolved fluorescence anisotropy decay measurement is necessary. Therefore, steady-state polarization alone cannot be used to study phase domains of cellular membranes with unknown compositions. In microscopy, the fluorescence intensity of a membrane probe not only is dependent on the local environment but is also dependent on its spatial orientation. Microscope optics have strong polarization artifacts. Therefore, fluorescence polarization measurements in microscopy require polarization calibrations.

We describe an alternative method for microscopy that features great simplicity and is based on the use of the GP function and two-photon excitation. This microscopic method may also provide three-dimensional information of membrane lipid phase states or order. The GP imaging method that we propose is the extension to microscopy of a well-established technique to study membrane structures and dynamics. The concept of GP was introduced by Parasassi et al. (1990) in the studies of lipid order of model systems using the membrane fluorescence probe Laurdan.

Laurdan is a naphthalene-based amphiphilic molecule (Weber and Farris, 1979). The quantum yield of Laurdan is much higher in membranes than in aqueous environments. Laurdan has low solubility in water. This strong partitioning increases background rejection for imaging cellular membrane structure. The fluorescence excitation and emission spectra of Laurdan are extremely sensitive to the polarity and to the dipolar dynamics of the environment (Parasassi et al., 1986). Laurdan shows relatively large emission spectral shifts in solvents of different polarity. This phenomenon is referred to as solvent relaxation, which originates from the reorientation of the solvent dipoles relative to the excited fluorescence probe molecules. Studies using phospholipid vesicles demonstrated that Laurdan is sensitive to the dynamics as well as to the polarity of the surrounding membrane. Therefore, Laurdan can distinguish whether a membrane is in a gel or a liquid-crystalline phase state (Parasassi et al., 1986). When Laurdan is in a lipid membrane it exhibits a 50-nm red shift of the emission spectrum as the membrane changes from gel into liquid-crystalline phase. The spectroscopic property, GP, can be used to measure this shift and to measures the rate of relaxation of water molecules in the membrane (Parasassi et al., 1994b). In fact, Laurdan GP has been found useful for numerous membrane studies (Parasassi et al., 1991; Levi et al., 1993; Fiorini et al., 1993).

GP bears the same functional form as conventional fluorescence polarization,

$$GP = \frac{I_b - I_r}{I_b + I_r},\qquad(1)$$

where I_b and I_r are the fluorescence intensities measured at the emission maxima (excitation GP) of Laurdan that are characterized by the gel and the liquid-crystalline phases, respectively. GP can also be measured from the excitation spectrum at fixed emission wavelength (emission GP). It is inconvenient to change the excitation wavelength of the laser system that we use. For this reason the emission GP is not used in the studies reported here. The emission maximum for the gel phase is at 440 nm and for the liquid-crystalline phase is at 490 nm.

There are several advantages of using GP compared with conventional fluorescence polarization. First, there is the possibility of acquiring the steady-state and dynamic information without polarizers. Second, GP provides a direct quantification of lipid membrane phase states including the calculation of fractions of different phase states in membranes with unknown lipid compositions (Levi et al., 1993). Third, GP can be measured in turbid media, which are often encountered in biological samples. Light scattering causes depolarization of both incident light and emitted fluorescence. For proper polarization or anisotropy measurements, this artifact must be corrected. The scattering contribution is not a problem for the GP measurement. In addition, for GP microscopy there is no need for a polarization correction for different objectives as well. All these advantages greatly simplify the measurement of GP, compared with fluorescence polarization, inside the microscope.

A disadvantage of fluorescence-intensity-based methods is that photobleaching can lead to measurement error. Laurdan is extremely susceptible to photobleaching. It is for this reason that Laurdan-labeled cell fluorescence imaging and GP measurement have not been successful in conventional confocal microscopy in which photobleaching is typically very large (Wells et al., 1989). However, the photobleaching effect can be largely reduced by the use of two-photon excitation (Denk et al., 1990), in which a fluorescent chromophore simultaneously absorbs two incident long-wavelength photons before it fluoresces. Two-photon excitation can be achieved by use of the very high peak power provided by a femtosecond pulsed laser (Denk et al., 1990). The advantages of two-photon fluorescence microscopy, compared with conventional microscopy, have been discussed in detail in the literature (Denk et al., 1995; Sandison et al., 1994).

To understand biological membranes better, we have to acquire knowledge from in situ studies of cells and studies of model systems. A variety of techniques, such as electron spin resonance (Sankaram et al., 1992), fluorescence photobleaching and recovery (Edidin and Stroynowski, 1991), differential calorimetry (Wolf et al., 1990), fluorescence digital imaging microscopy (Rodgers and Glaser, 1993),

and near-field microscopy (Hwang et al., 1995) as well as fluorescence spectroscopy (Parasassi et al., 1993b), have been applied to membrance studies. The studies of structure and function of biological membranes using Laurdan GP in the past few years have been very fruitful (Parasassi et al., 1992, 1993a; Levi et al., 1993). In the following section we discuss some examples of current problems concerning membrane composition and heterogeneity that can be studied by the methodology developed here.

In living cells the saturation of fatty acids and the cholesterol content vary with time and with the specific type of membrane, which may provide differences in membrane fluidity and functions (Quinn et al., 1989). For instance, in the study of stress response of cellular membrane it has been found that, on cooling, the fluidity of the plasma membrane increases as the result of increased production of more unsaturated fatty acid (Maresca and Cossins, 1993). Vigh et al. (1993) have also shown that, by modifying the fatty acid in the plasma membrane of yeast cells, they were able to stimulate the synthesis of unsaturated fatty acid. There are many questions associated with these observations: Can membranes act as fluidity sensors in general and in all cell types, or are the sensors specifically linked with the plasma membrane? How does the sensor function at a molecular level? Before addressing these questions, we would like to know whether there are any differences in membrane fluidity of living cells and what the local variations are. Of particular interest are the plasma membrane and the nuclear membranes. For eukaryotic cells the plasmam embrane is the outer most structure, which controls the flow of material, flow of energy, and flow of information from the exterior of the cell. Nuclear membranes, on the other hand, are the ultimate communication channel between the nucleus and the rest of the cell. In general, the structure, organization, and chemical composition of the plasma and nuclear membranes are different (Evans and Graham, 1989). An important fact to uncover is whether the difference in lipid composition of the two membranes can be observed as a difference of fluidity or phase state. To our knowledge, there is still no conclusive experimental evidence showing a difference in fluidity or membrane phase state of these membranes simultaneously in living cells. Fluorescence polarization microscopy is a quantitative way to assess cellular membrane fluidity and its local variation. As we have mentioned above, the measurement of fluorescence polarization in a microscope has practical disadvantages. Instead, the GP method that we describe provides a similar level of quantitative information and is practical to implement in the fluorescence microscope. Here we illustrate, with a series of examples, the implementation of the GP method in the two-photon microscope. We found that the GP values are broadly distributed in living cells, and we found significant GP differences among different membranes and in different locations of the same membrane. We also discuss possible measurement artifacts that are due to autofluorescence and lifetime quenching by other cellular components.

MATERIALS AND METHODS

Two-photon scanning fluorescence microscope for Laurdan GP and lifetime measurements

A two-photon scanning fluorescence microscope has been developed in our laboratory (So et al., 1995). This microscope has the capability of both steady-state and fluorescence-lifetime-resolved imaging. For generalized polarization measurement, minor modifications have been applied to the previous system. The instrument setup is presented in Fig. 1.

A Ti–sapphire laser (Mira 900, Coherent Inc., Palo Alto, CA) pumped by an Ar-ion laser (Innova 310, Coherent Inc., Palo Alto, CA) is used as the excitation light source. The Ti–sapphire laser is a very stable light source, providing intensity fluctuations of less than 0.5%. The wavelength of the laser was tuned to 770 nm, where it has the maximum power. This wavelength is suitable for Laurdan two-photon excitation at an equivalent one-photon excitation of 385 nm.

The laser light is guided by a galvanometer-driven X–Y scanner (Cambridge Technology, Watertown, MA) to achieve beam scanning in both X and Y directions. The scanner is controlled by the data acquisition computer via a custom-built interface circuit. A signal coming from the main computer sequentially triggers each step of the raster scan from the upper left to the lower right corner of the sampling region (256 × 256 pixels). The maximum scan rate of the scanner is 500 Hz over a range of ±60° for both the X and the Y mirrors. At the maximum frequency a frame rate of less than 0.5 s could be achieved. At this rate the pixel residence time would be less than 8 μs. To reduce photon noise we typically increase the pixel residence time to 320 μs, resulting in a frame rate of ~0.5 min. A 200-kHz signal from a frequency synthesizer (Hewlett-Packard, Inc., Santa Clara, CA) is sent to the data acquisition computer so that it may synchronize the scan rate with the external sources. A scan lens in the epiluminescence light path of the inverted microscope (Zeiss Axiovert 35, Zeiss, Inc., Thronwood, NY) linearly translates the angular motion of the input beam from the scanner to lateral displacements at the back focal plane of the microscope objective. The laser power is attenuated by a polarizer to approximately 20–30 mW before input to the microscope. The sample receives ~10% of the incident power. A quarter-wave plate (CVI Laser Corporation, Albuquerque, NM) is placed after the polarizer to change the polarization of the laser light from linear to circular.

The Z position can be controlled by a stepper motor coupled to the manual height adjustment knob of the microscope. The Z position is monitored by a linear variable differential transformer (Schaevitz Engineering, Camden, NJ). A single-board computer (8052 microprocessor, Iota System, Inc., Incline Village, NV) actively reads the position of the linear variable differential transformer and controls the motion of the stepper motor. With our current system an accuracy of 200 nm in the Z position can be achieved.

The dichroic mirror (Chroma Technology, Inc., Brattleboro, VT) reflects the excitation beam to the sample and passes the fluorescence. Two optical bandpass filters (Ealing Electro-Optics, New Englander Industrial Park, Holliston, MA), with 46-nm bandwidth and centers at 446 and 499 nm are used to collect fluorescence at the red and blue edges of the Laurdan emission spectrum. In practice, the two filters are exchanged each time a full frame has been scanned. To compensate for photobleaching, three successive pictures in a sequence of red–blue–red are collected, and the two red pictures are averaged. The filters are mounted upon a motor-driven sliding device in the microscope. A short-pass filter is also used to eliminate further the residual excitation light. For the GP measurement, a 10-cm-long liquid filter filled with a Cu_2SO_4 solution and having an ~20 o.d. at the excitation wavelength acts as the barrier filter. This filter passes 90% of the fluorescence at wavelengths below 600 nm. The fluorescence is detected by a cooled R1104 photomultiplier tube (Hamamatsu, Bridgewater, NJ).

To investigate possible GP artifacts in the two-photon microscope we measured the fluorescence lifetime of the Laurdan-labeled cell. We used the instrument configuration previously described (So et al., 1995). In contrast to Piston et al. (1992), we base our lifetime-resolved
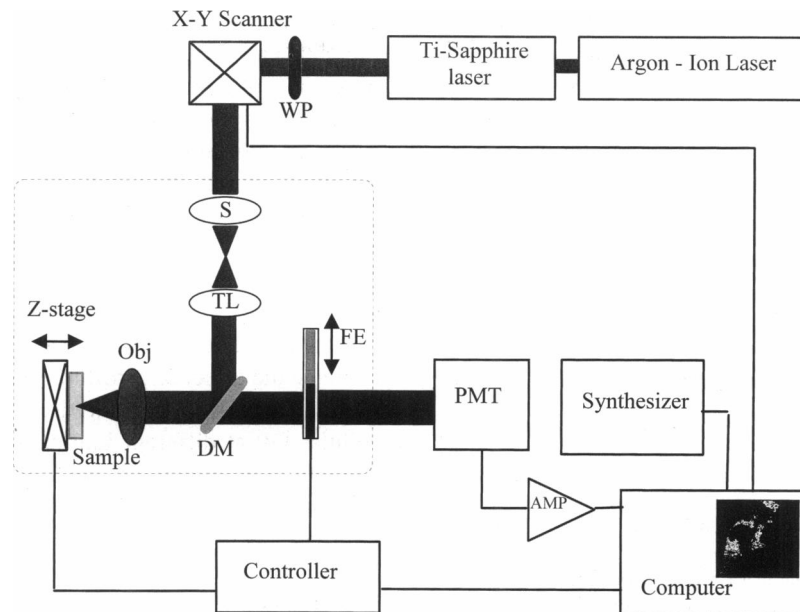
FIGURE 1 Schematic of the scanning two-photon fluorescence microscope: WP, quarter-wave plate; S, scan lens; TL, tube lens; DM, dichroic mirror; Obj, microscope objective; FE, filter exchanger. Two bandpass filters centered at ~440 and ~490 nm have been used to obtain the blue and red edges of Laurdan fluorescence intensity images. Scanning in the Z direction is achieved by changing the position of the focal plane on the sample. The focal plane position is controlled by a custom-made feedback controller that makes use of a linear variation differential transformer. The components within the dashed box are inside the microscope. The whole instrument is centrally controlled by a main computer (see text for details).

scanning microscope on a pixel-by-pixel measurement rather than on combining several frames. The lifetime instrument is practically the same as the GP instrument, except for the addition of electronics for frequency-domain data acquisition. The Ti–sapphire laser self-mode locks at 80 MHz (i.e., the modulation frequency f), which is useful for measuring lifetimes of several nanoseconds. With a 25-kHz cross-correlation frequency, the signal was sampled at 100 kHz and averaged in time for four cross-correlation waveforms (four times folding), resulting in a pixel residence time of 160 μs. To reduce background noise further, three to five frames of data were averaged. Because of the stability of the Ti–sapphire laser, only a single data acquisition channel of the 12-bit A2D card (A2D-160, DRA Laboratories, Sterling, VA) was used. The lifetime reference was a 2-mM fluorescein–water solution ($\tau = 4$ ns). A reference lifetime image was collected after each Laurdan lifetime image.

Cell labeling with Laurdan

Laurdan-cell-labeling procedures are simplified from those previously described (Parasassi et al., 1992). Mouse fibroblast cells (ATCC CRL 1503 mouse embryonic fibroblast) subcultured in Dulbecco's minimum essential medium (DMEM) were kindly provided by the Institute of Animal Research, University of Illinois at Urbana-Champaign. For microscopy studies the mouse fibroblast cells were grown on microscope slide cover glass. Usually there were ~10^5 cells on a 2.5 $\times$ 2.5 cm^2 cover glass. Laurdan labeling was performed directly in the cell culture media. 10 ml of Laurdan (Molecular Probes, Inc., Eugene, OR) stock solution was added per milliliter of DMEM. The stock Laurdan solution concentration was ~1 mM in dimethyl sulfoxide (Me$_2$SO; Sigma, St. Louis, MO), and it was renewed every three weeks. After 30 min of incubation in the dark at room temperature, the cover glass was washed once with DMEM and mounted upon a hanging drop microscope slide.

Imaging analysis

GP and intensity images

Different Z-section images of a cell are considered as a single group. We obtain the GP images from the intensity images by calculating the GP for each pixel, using Eq. 1. The normalized variance image, N, is obtained as follows:

$$N_i = \left| \frac{P_i - \bar{P}}{\bar{P}} \right|, \qquad (2)$$

where P_i is any valid pixel value of the image and N_i is the normalized value at that pixel and $\bar{P}$ is the averaged value of all valid pixels of the image. The normalized variance image allows us to inspect the fluctuation of either intensity or GP values around the average. A pixel is valid when any of the values at the same pixel position of the set of red–blue–red images is larger than a threshold. The threshold is picked to give a clear contrast of the GP image from the background. Single-value correlations between GP and intensity images for both red and blue were also studied. The correlation imaging, C, was obtained as follows:

$$C_i = \frac{GP_i - \overline{GP}}{\overline{GP}} \frac{I_i - \bar{I}}{\bar{I}}, \qquad (3)$$

where $\overline{GP}$ and $\bar{I}$ are the average values of any group of GP and intensity images, respectively, and I_i and C_i are the pixel values in the intensity and correlation images, respectively.

Imaging of Laurdan fluorescence lifetime

In the frequency domain, the modulation frequency f (for both light source and detection PMT), the phase shift ϕ (i.e.,

the phase difference between the fluorescence and the excitation light), the modulation factor M, and the fluorescence lifetime τ have the following relationship for a single exponential decay (Gratton and Limkeman, 1983):

$$\tan(\phi) = 2\pi f\tau, \tag{4}$$

$$M = \frac{1}{\sqrt{1 + (2\pi f\tau)^2}}. \tag{5}$$

Therefore, the absolute phase ϕ and modulation M values of the sample can be obtained from

$$\phi = (\phi_s - \phi_r) + \arctan(2\pi f\tau_r), \tag{6}$$

$$M = \frac{AC_s/DC_s}{AC_r/DC_r} \frac{1}{\sqrt{1 + (2\pi f\tau_r)^2}}. \tag{7}$$

where DC is the intensity image and AC is the ac component of the intensity-modulated image. The subscripts s and r stand for sample and reference, respectively. Assuming that Laurdan fluorescence decay is also a single exponential, its lifetime can easily be calculated from Eqs. 4 and 5.

RESULTS AND DISCUSSION

Cellular fluorescence intensity and GP images

Living cells have autofluorescence mainly from reduced nicotinamide adenine dinucleotide and flavoprotein (Giordano et al., 1993; Sewell and Mroz, 1993). With a two-photon scanning microscope Webb and co-workers were able to use cell autofluorescence to study cellular activities (Williams et al., 1994). For the purpose of obtaining the GP image, autofluorescence is a source of error and requires correction. There are two ways to get around this problem. First, the Laurdan labeling concentration can be increased, so that the Laurdan fluorescence is significantly greater than the autofluorescence. Second, the autofluorescence intensity fraction can be measured or calculated and removed. The

second method is more difficult to achieve in practice than the first one because the intensity of cellular autofluorescence is not uniform (Williams et al., 1994). To obtain spatially correlated autofluorescence images, one must measure the autofluorescence on the same cell that will be labeled with Laurdan. The lifetime difference between the autofluorescence and Laurdan fluorescence is very distinct. In principle, the fraction of autofluorescence can also be calculated from Laurdan-labeled cell images. This procedure requires dedicated measurements and data analysis. For the above reasons we have chosen the first method. To estimate the effect of autofluorescence and determine which Laurdan labeling concentration to use, we measured the cellular GP at different Laurdan concentrations as well as the autofluorescence from the same well of cells, using our two-photon microscope. Average GP values at different Laurdan-labeling concentrations with and without correction for the average autofluorescence are plotted in Fig. 2. We obtained the GP value at each point by averaging all valid pixels in each image. Four to five frames were averaged, and there were ~10,000 valid pixels in each frame. Clearly, without autofluorescence correction the general trend of cell GP values decreases with decreasing Laurdan-labeling concentration. After correction the average GP values are ~0.3, independent of Laurdan concentration, as it should be. For the cellular GP imaging we chose a Laurdan concentration (10 μM) that was high enough that any autofluorescence correction would be insignificant.

Laurdan-labeled cellular fluorescence intensity images are shown in Fig. 3(A and B). Evidently, the distribution of Laurdan is not uniform for both edges of the Laurdan emission spectrum. For most of the cells that we examined, the major intensity-enriched domains are close to the nuclear cleft, i.e., the areas between the arrow pairs indicated in Fig. 3 (A and B). From the cell morphology, the fluorescence-enriched domain could be cell organelles such as the

FIGURE 2   Averaged GP values as a function of Laurdan-labeling concentration with (a) and without (b) autofluorescence correction. Four to five images were averaged for each data point. The typical error for each GP point is smaller than 0.02. All measurements were done with the same well of cells. For the images presented in this work, 10 μM of final Laurdan concentration was used to label the cells so that the autofluorescence would have a negligible effect on the GP images.
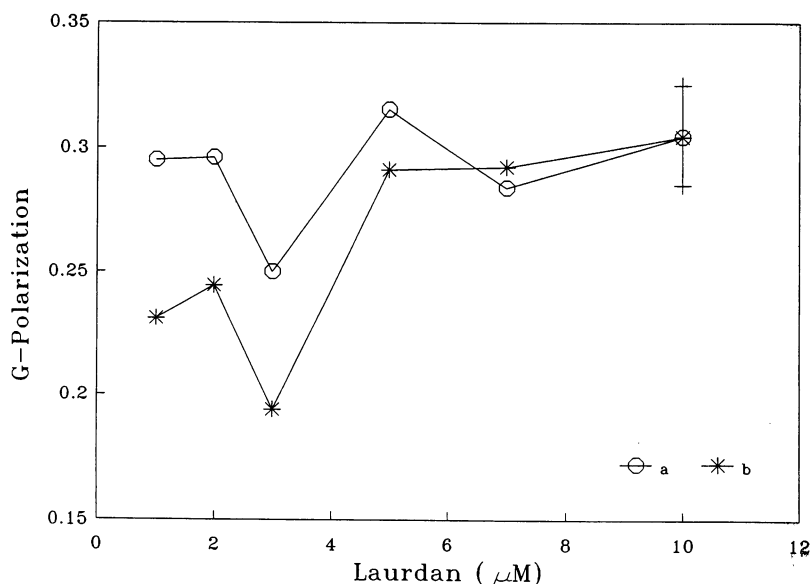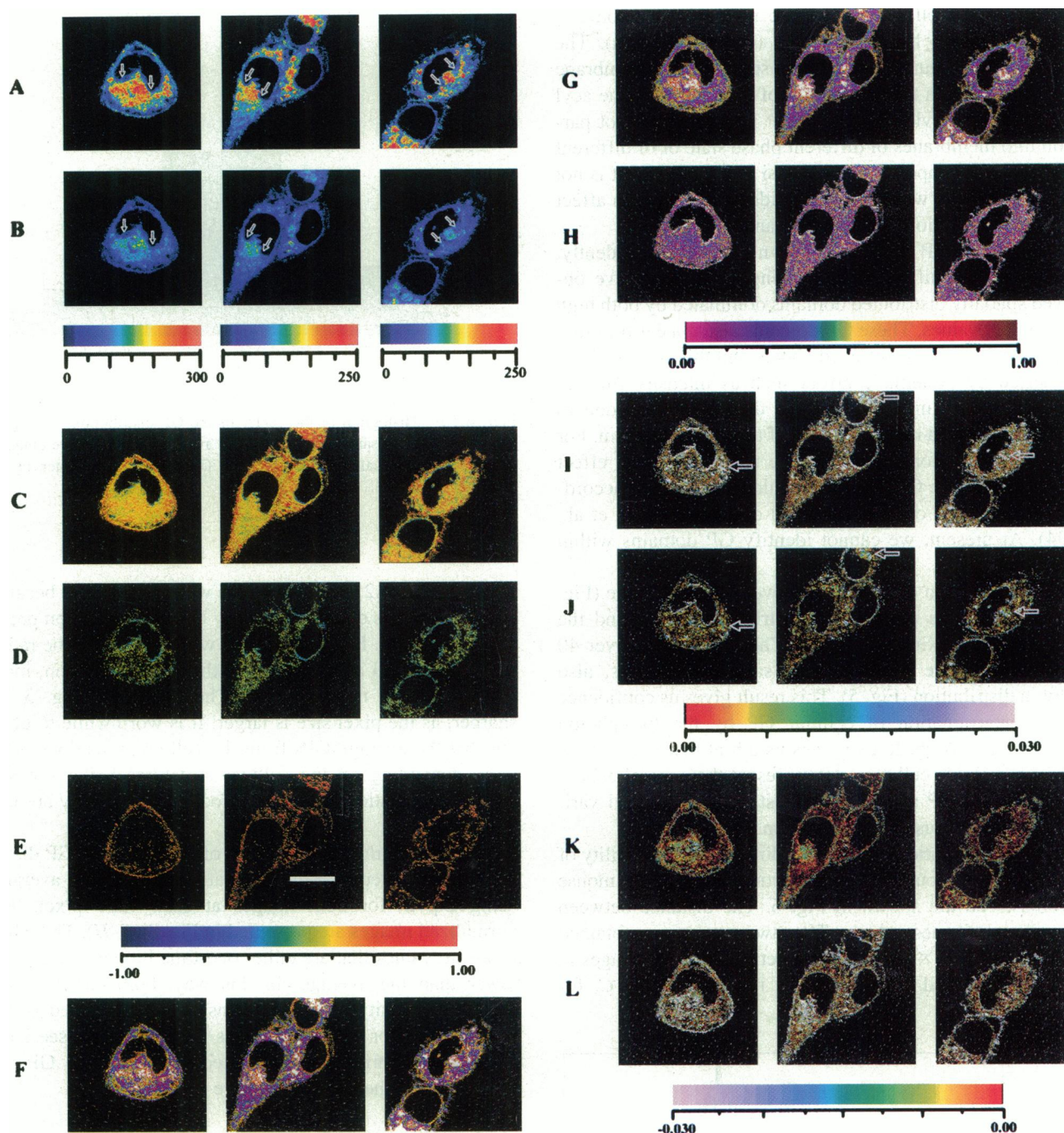
FIGURE 3 Examples of three different *X–Y* image sections of mouse fibroblast cells labeled with Laurdan. The fibroblast cells were grown on a microscope slide cover glass and directly labeled in the growth medium DMEM. The measurement was performed at room temperature. An averaged laser excitation power of approximately 2–3 mW after the microscope objective (Zeiss 63 × 1.25 N.A. oil emulsion) was used. Series A and B are the intensity images of different cells as seen through the blue and red bandpass filters, respectively. Series C are the corresponding GP images. In series D, GP values smaller than 0.2 are plotted. In Series E, GP values greater than 0.5 are plotted. Series F–H are images of the absolute fluctuations of intensities (*A* and *B*) and GP (*C*) around their average values. Series I and J are positive correlation images between A and C, and B and C, respectively. Series K and L are images of negative correlations between A and C, and B and C, respectively. In A and B the areas close to the nuclear cleft as indicated between the arrows in each cell often associate with the main intensity domains. In I and J some areas of both high intensity and high GP are indicated by arrows. The scale bar is 10 μm.

Golgi apparatus, endoplasmic reticulum, and mitochondria. There are still very few studies of living cells labeled with Laurdan. From the limited knowledge that we have, we may speculate that the intensity distribution may arise from i)

cells that actively enrich Laurdan into certain regions or ii) Laurdan passively partitioned into cellular membranes because of the differences in their lipid compositions. We have also observed these kinds of Laurdan intensity domain in

other types of cell such as mouse macrophage, mouse T cells, and mouse hybridoma cells (data not shown). The position of the Laurdan molecule inside the lipid membrane is such as to align the lauroyl tail of Laurdan with the acyl chains. It was peviously found that Laurdan does not partition into membranes of different phase state or of different phospholipid composition (Parasassi et al., 1993b). It is not known, however, whether other lipids or proteins can affect Laurdan distribution in the membrane.

Examples of GP images are shown in Fig. 3 *C*. Evidently, the GP is not uniform within a single cell. We have observed spatially distributed domains dominated by both high and low GP values. These GP domains also appear for other types of cell, as we mentioned above, and this is unlikely to be caused by systematic errors such as intensity fluctuations. It is also unlikely that the differences are due to different localized heating effects of the scanning beam. For the small excitation power that we use, the heating effect that would induce GP changes should be negligible according to the results of Tromberg and co-workers (Liu et al., 1994). At present, we cannot identify GP domains within cell organelles.

The distribution of GP values covers a broad range (Fig. 4). Typically, the peak of the distribution is 0.3 and the width at half-maximum is ~0.5. The average GP over 40 cells, which were grown on the same cover glass, also shows a distribution (Fig. 5). This result gives us confidence in the determination of cellular GP by the two-photon excitation approach. It also gives us a hint that the average GP from a single cell may not represent the general behavior of cellular GP and that we must account for cell variability when discussing results from a single cell.

As a demonstration of the three-dimensional capability of our instrument, four GP image sections of a single mouse fibroblast cell are shown in Fig. 6. The distance between two adjacent frames is 1 μm. The raw images were obtained with a Zeiss 100 $\times$ 1.25 N.A. objective. The GP images in Fig. 6 are blurred compared with those in Fig. 3 *C*, for
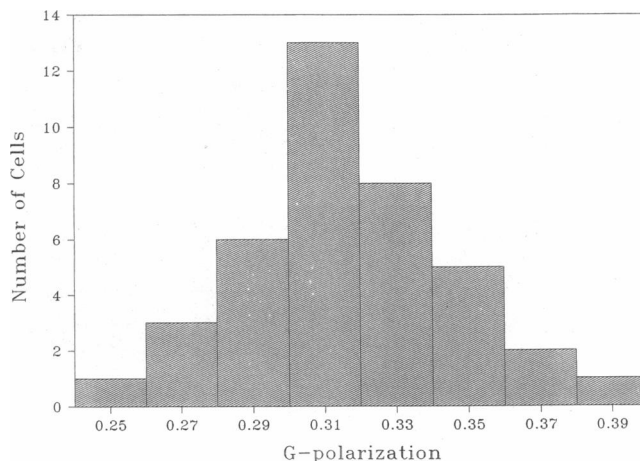
FIGURE 5   Histogram of the center of the GP distributions among 40 cells grown on the same cover glass. The average GP values are obtained by averaging all valid pixels for each GP image. The center of the distribution is ~0.3.

which a 63 $\times$ 1.25 N.A. objective was used. This is because our resolution is defined primarily by the two-photon point-spread function. For an objective with 1.25 N.A., the radial resolution is 0.3 and 0.9 μm for the axial resolution, independent of the magnification. The images in Fig. 3 are sharper, as the pixel size is larger. It is worthwhile to point out that the average GPs from the cell cross sections often vary, depending on the cellular structures being imaged. The GP fluctuations around the focal plane usually are less than 10%.

To compare the heterogeneity of intensity and GP distributions, we calculated the fluctuations around the average, using Eq. 2, for both images at each valid pixel. The normalized images are presented in Fig. 3 (*F–H*). The white areas are values that are either one-time higher or one-time lower than the average. In this way, both enriched and depleted intensity or GP domains will be included in the white areas. For intensity images we can clearly see large fluorescence-enriched or -depleted domains. The GP images, on the other hand, are more uniform.

GP value reflects membrane fluidity

The relaxation rate of the excited states of Laurdan molecule, which is measured by the GP value, depends on the local dynamics of water molecules in the membrane (Parasassi et al., 1994b). The absence of relaxation is generally associated with the absence of water. In this sense, GP differences are related to the "fluidity" as sensed by the water molecules. Numerous studies of model systems have determined that the GP value is independent from the type of phospholipid (Parasassi et al., 1991, 1993b, 1994a). Instead, the crucial factor affecting the GP is the local membrane packing that allows water to penetrate the membrane and to relax around the excited Laurdan molecule. The GP
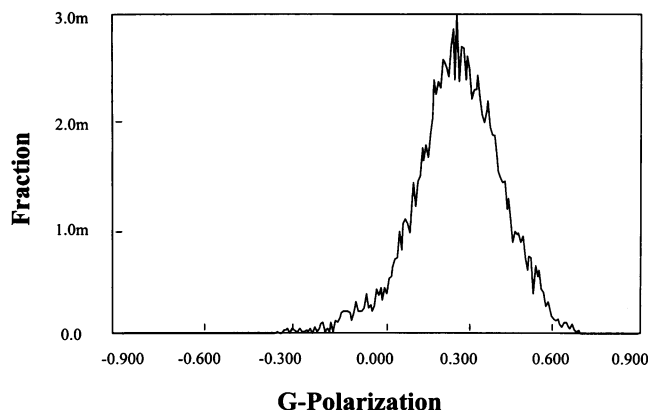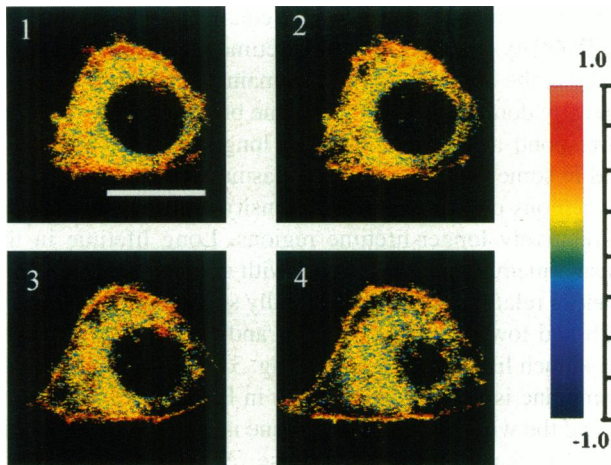

FIGURE 4   Typical distribution of generalized polarization from an image of a single mouse fibroblast cell labeled with Laurdan. The fraction of pixels from the total pixel number of a single frame is plotted along the ordinate (m stands for milli), and GP is plotted along the abscissa.

FIGURE 6　Four GP cross sections of a single mouse fibroblast cell labeled with Laurdan. The distance between subsequent frames is 1 μm. A 100 × 1.25 N.A. oil immersion Zeiss objective was used. The laser pixel dwell time is ~300 μs. Features of GP domains can be seen. The scale bar is 10 μm.

images in Fig. 3 C, thus, are a map of membrane fluidity in different cellular structures. Smaller GP values indicate higher membrane fluidity and vice versa.

GP and cellular membrane structures

By examining hundreds of cell GP images, we noticed that high-GP regions can be found more often on the plasma membrane. On the other hand, low-GP regions more often associate with the nuclear membranes. This phenomenon is found, for example, in Fig. 3 C. On the plasma membrane there are more red-colored areas than on the nuclear membranes, whereas there are more green- and blue-colored areas on the nuclear membranes than on the plasma membrane. This scenario is clearly seen from the digitally separated GP images (Fig. 3 D and E). Red color indicates high GP, and green color indicates low GP. In Fig. 3 E the plasma membrane is clearly visible, but not the nuclear membranes; whereas in Fig. 3 D the nuclear membranes are more visible than the plasma membrane. When one simply looks at the intensity images (Fig. 3 A and B), the plasma membrane and the nuclear membranes are almost featureless. From previous studies it is know that, usually when the lipid membrane is in the gel phase (Parasassi et al., 1991), has high cholesterol content (Parasassi et al., 1994a), or both, GP has high values (Gp > 0.5), and when the lipid membrane is in the liquid-crystalline phase state or has a low cholesterol content, GP has lower values (Gp < 0.2 when more than 80% of the lipids are in the liquid-crystalline phase state) (Parasassi et al., 1993b). Usually, plasma membrane is known to have the highest cholesterol fraction among cellular membranes and the nuclear membranes have the least amount of cholesterol (Evans and Graham, 1989).

The differences in the cholesterol content could be one simple explanation for the observed GP differences. We notice that even on the plasma membrane or the nuclear membranes the GP values are also distributed. Using image edge deconvolution methods, we estimated the average GP values on the plasma and nuclear membranes. For cells in Fig. 3 C the average GP on plasma membrane is ~0.41 (±0.03) and on nuclear membranes the average GP is ~0.21 (±0.03). The full width at half-maximum of the GP distribution for both membranes of a single cell is ~0.4, slightly smaller than the GP distribution for the whole cell. The GP variations between the plasma membrane and the nuclear membranes are significant. Neighboring pixels typically have a GP noise less than 0.1 from our measurement. This noise level is smaller than the average GP difference found between the plasma membrane and the nuclear membranes. This heterogeneity in GP could also indicate coexistence of membrane lipid phase domains. It has been found that cellular membrane domains, as well as lipid compositions, are intimately related to many biological processes such as protein biogenesis, cell motility, and signal transmission (Singer, 1990; Stossel, 1993; Divecha and Irvine, 1995).

Correlation between the GP and intensity images

Although the GP images are calculated from the intensity images, it is still helpful to know whether there are any correlations between the two quantities. In Fig. 3 I–L single-point correlation images between intensity and GP are shown. Positive correlation means that the intensity changes of the cell membranes follow the changes of GP. Negative correlation means that the intensity and the GP change in opposite directions. By close examination of the images we found that certain regions of high intensity are positively correlated with high GP and vice versa. For example, the areas marked with arrows in Fig. 3 I and J are high in intensity and GP. For the nuclear membranes the positive correlation is clearly shown in light colors. Referring to the intensity (Fig. 3 A and B) and GP (Fig. 3 C) images, the nuclear membranes are low in both intensity and GP. On the other hand, from the negative correlation images (Fig. 3 K and L) we find that some of the brightest regions in the intensity images are negatively correlated with the GP. At present we cannot answer the question of why in certain cases intensity and GP are positively correlated and in other cases they are negatively correlated. We also do not know the reason for the large GP distributions. Probably there is not a simple relationship between intensity and GP of Laurdan-labeled lipid membranes. It is likely that intensity depends on enrichment of Laurdan into local membranes because of different chemical compositions of the membrane, whereas GP is an intrinsic property of the lipid phase state.
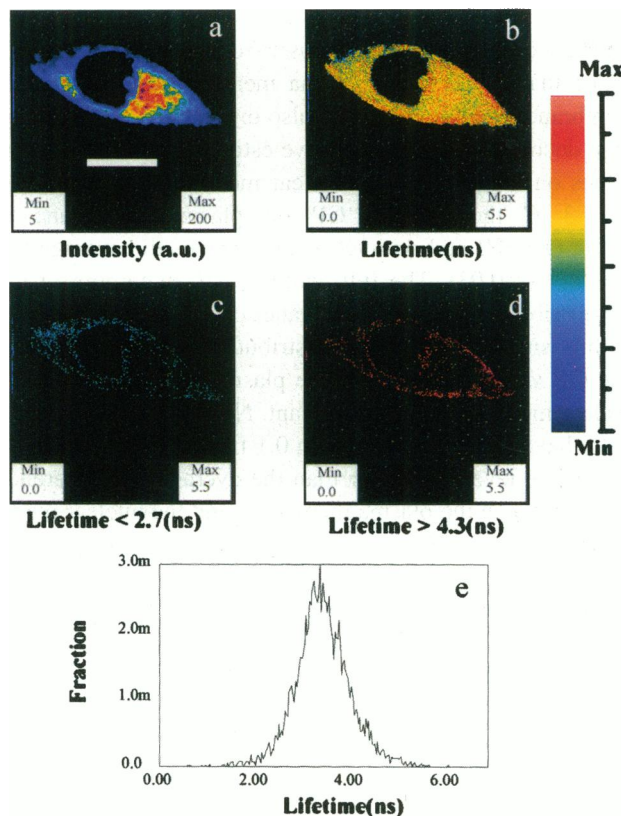
FIGURE 7   Intensity and fluorescence lifetime images of Laurdan-labeled mouse fibroblast cell: (a) the intensity, (b) the lifetime, (c) regions with lifetime $\tau > 2.7$, (d) regions with lifetime $\tau < 4.3$, (e) distribution of the lifetime. It is evident that regions with $\tau > 4.3$ are strongly associated with the plasma membrane, whereas the nuclear membranes and some other parts of the cell preferentially display with $\tau < 2.7$. The raw images were collected from a 63 × 1.25 N.A. Zeiss objective. The scale bar is 10 μm.

Lifetime images

Another concern about the heterogeneity of GP distribution is whether the GP distribution is caused by a localized quenching effect, because the GP value depends on the lifetime. There are many substances that may quench the fluorescence of Laurdan inside the cell. For example, heme and flavin are quite abundant, and their absorption spectrum largely overlaps Laurdan emission spectra. Oxygen is also a well-known fluorescence quencher. To examine the possibility of such bias, we measured the fluorescence lifetime of Laurdan-labeled cells by using two-photon time-resolved microscopy. The intensity and calculated lifetime images are presented in Fig. 6. The Laurdan lifetime image data fit well to a single exponential decay. The center of the lifetime distribution is ~3.5 ns, and the width at half-maximum is ~1.0 ns (Fig. 7e). Evidently, the lifetime distribution is also not uniform (Fig. 7). We can recognize localized domains with either high or low lifetimes. If these domains are caused solely by quenchers, then the variation of lifetime should follow the variation of intensity, when only steady-

state and dynamic quenching are considered. By comparing the intensity (Fig. 7 A) and the lifetime (Fig. 7 B) images we find that the observed lifetime domains do not correlate with intensity domains. For instance, the brightest regions do not correspond to the domains with longer lifetimes. We also find in some areas close to the plasma membrane that there are regions of relatively low intensity, but they correspond to relatively longer-lifetime regions. Long lifetime in the plasma membrane is consistent with the idea that the membrane is relatively rigid. By digitally separating regions with high and low lifetimes (Fig. 7 C and D) we obtain images very much like the GP images (Fig. 3 D and E). The plasma membrane is more clearly shown in Fig. 7 D than in Fig. 7 C, and the whole nuclear membrane is more recognizable in Fig. 7 C than in Fig. 7 D. These results suggest that the quenching effects may not be significant enough to bias the GP measurements and that the lifetime domains may very well be the same as GP domains. It is also worthwhile to mention that lifetime imaging is technically more complex than intensity-based GP imaging.

CONCLUSIONS

To study cell membranes we have developed a protocol capable of measuring Laurdan GP images based on two-photon microscopy. The feasibility of the method was demonstrated with examples, and the results of the measurements were discussed. For correct cellular GP measurement the autofluorescence effect needs to be considered. From the intensity images we observed that there were Laurdan-enriched fluorescence domains. In other words, Laurdan is not evenly distributed in cellular membranes. We also observed that the GP images were not uniform among different membranes in the same cell and on the same membrane. In comparing the intensity and GP images we found no simple correlations between the two. This result suggests that the intensity and the GP are independent and that the differential partitioning effect of Laurdan into cellular compartments is unlikely due to the differences in lipid membrane phase states. On the other hand, we are able to separate digitally the cellular compartments that are either high or low in GP. We found that regions on the plasma membrane often display high GP and regions on the nuclear membranes display low GP. As GP value reflects membrane fluidity, we conclude that the plasma membrane is relatively rigid and that nuclear membranes, on the other hand, are more fluid. The heterogeneity in GP is much greater than our measurement error. We believe that the distribution is caused by differences, such as polarity, lipid compositions, or lipid phase state, in the local probe environment.

REFERENCES

Aloia, R. C., H. R. Tian, and F. C. Jensen. 1993. Lipid composition and fluidity of the human immunodeficiency virus envelope and host cell plasma membranes. *Proc. Natl. Acad. Sci. USA.* 90:5181–5185.

Blumenthal, R., C. C. Pak, Y. Raviv, M. Krumbiegel, L. D. Bergelson, S. J. Morris, and R. J. Lowy. 1995. Transient domains induced by influenza haemagglutinin during membrane fusion. *Mol. Membr. Biol.* 12:135–142.

Denk, W., D. W. Piston, and W. W. Webb, 1995. Two-photon molecular excitation in laser-scanning microscopy. *In* Handbook of Biological Confocal Microscopy. J. B. Pawley, editor. Plenum Press, New York, 445–458.

Denk, W., J. H. Strickler, and W. W. Webb. 1990. Two-photon laser scanning fluorescence microscopy. *Science.* 248:73–76

Divecha, N., and R. Irvine. 1995. Phospholipid signaling. *Cell.* 89:269–278.

Edidin, M., and I. Stroynowski. 1991. Differences between the lateral organization of conventional and inositol phospholipid-anchored membrane proteins. A further definition of micrometer scale membrane domains. *J. Cell Biol.* 6:1143–1150.

Evans, W. H., and J. M. Graham. 1989. *In* Membrane Structure and Functions. D. Richwood and D. Male, editors. IRL Press, Eynsham, Oxford, England. 1–82.

Fiorini, R., G. Curatola, A. Kantar, P. L. Diorgi, and E. Gratton. 1993. Use of Laurdan fluorescence in studying plasma membrane organization of polymorphonuclear leukocytes during the respiratory burst. *Photochem. Photobiol.* 57:438–441.

Florine-Casteel, K. 1990. Phospholipid order in gel- and fluid-phase cell-size liposomes measured by digitized video fluorescence polarization microscopy. *Biophys. J.* 57:1199–1215.

Gicquaud, C., and P. Wong. 1994. Mechanism of interaction between actin and membrane lipids—a pressure-tuning infrared spectroscopy study. *Biochem. J.* 303:769–774.

Giordano, E., V. Cirulli, D. Bosco, D. Rouiller, P. Halban, and P. Meda. 1993. B-cell size influences glucose-stimulated insulin secretion. *Am. J. Physiol.* 265:C358–C364.

Gordon, G. W., B. Chazotte, X. F. Wang, and B. Herman. 1995. Analysis of simulated and experimental fluorescence recovery after photobleaching—data for two diffusing components. *Biophys. J.* 68:766–778.

Grant, C. W. M. 1983. Lateral phase separations and the cell membrane. *In* Membrane Fluidity in Biology, Vol. 2. R. C. Aloia, editor. Academic Press, New York. 131–150.

Gratton, E., and M. Limkeman. 1983. A continuously variable frequency cross-correlation phase fluorometer with picosecond resolution. *Biophys J.* 44:315–324

Hwang, J. S., C. Bohm, L. Tamm, E. Betzig, and M. Edidin. 1995. Nanoscale complexity of transferred monolayers studied by near-field scanning optical microscopy. *Biophys. J.* 68:A293

Jajoo, A., A. Dube, and S. Bharti, 1994. Mg^{2+}-induced lipid phase transition in thylakoid membranes is reversed by anions. *Biochem. Biophys. Res. Commun.* 202:1724–1730.

Lentz, B. R. 1988. Membrane "fluidity" from fluorescence anisotropy measurements. *In* Spectroscopic Membrane Probes, Vol. I. L. M. Loew, editor. CRC Press, Inc., Boca Raton, FL. 13–41.

Levi, M., P. V. Wilson, O. J. Cooper, and E. Gratton. 1993. Lipid phases in renal brush border membranes revealed by Laurdan fluorescence. *Photochem. Photobiol.* 57:420–425.

Liu, Y., D. K. Cheng, G. J. Sonek, M. W. Berns, and B. J. Tromberg. 1994. Microfluorometric technique for the determination of localized heating in organic particles. *Appl. Phys. Lett.* 85:919–921.

Maresca, B., and A. R. Cossins. 1993. Cell physiology—fatty feedback and fluidity. *Nature (London).* 365:606–607.

McElhaney, R. N. 1985. Membrane lipid fluidity, phase state, and membrane function in prokaryotic microorganisms. *In* Membrane Fluidity in

Biology, Vol. 4. R. C. Aloia and J. M. Boggs editors. Academic Press, New York. 147–208.

Paller, M., S. 1994. Lateral mobility of Na, K-ATPase and membrane lipids in renal cells—importance of cytoskeletal integrity. *J. Membr. Biol.* 142:127–135.

Parasassi, T., F. Conti, and E. Gratton. 1986. Time-resolved fluorescence spectra of Laurdan in phospholipid vesicles by multifrequency phase and modulation fluorometry. *Cell. Mol. Biol.* 32:103–108.

Parasassi, T., G. De Stasio, A. d'Ubaldo, and E. Gratton. 1990. Phase fluctuations in phospholipid membranes revealed by Laurdan fluorescence. *Biophys. J.* 57:1179–1186.

Parasassi, T., G. De Stasio, G. Ravagnan, R. M. Rusch, and E. Gratton. 1991. Quantitation of lipid phase in phospholipid vesicles by the generalized polarization of Laurdan fluorescence. *Biophys. J.* 60:179–189.

Parasassi, T., M. Di Stefano, M. Loiero, G. Ravagnan, and E. Gratton. 1994a. Influence of cholesterol on phospholipid bilayers phase domains as detected by Laurdan fluorescence. *Biophys. J.* 66:120–132.

Parasassi, T., M. Di Stefano, M. Loiero, G. Ravagnan, and E. Grattan. 1994b. Cholesterol modifies water concentration and dynamics in phospholipid bilayers: a fluorescence study using Laurdan probe. *Biophys. J.* 66:763–768.

Parasassi, T., M. Di Stefano, G. Ravagnan, O. Sapora, and E. Gratton. 1992. Membrane aging during cell growth ascertained by Laurdan generalized polarization. *Exp. Cell Res.* 202:432–439.

Parasassi, T., M. Loiero, M. Raimondi, G. Ravagnan, and E. Gratton. 1993a. Absence of lipid gel-phase domains in seven mammalian cell lines and in four primary cell types. *Biochim. Biophys. Acta.* 1153:143–154.

Parasassi, T., G. Ravagnan, R. M. Rusch, and E. Gratton. 1993b. Modulation and dynamics of phase properties in phospholipid mixtures detected by Laurdan fluorescence. *Photochem. Photobiol.* 57:403–410.

Piston, D. W., D. R. Sandison, and W. W. Webb. 1992. Time-resolved fluorescence imaging and background rejection by two-photon excitation in laser scanning microscopy. *In* Time-Resolved Laser Spectroscopy in Biochemistry III, *Proc. Soc. Photo-Opt Instrum. Eng.* 1640:379–389.

Quinn, P. J., F. Joo, and L Vigh. 1989. The role of unsaturated lipids in membrane structure and stability. *Prog. Biophys. Molec. Biol.* 53:71–103.

Rodgers, W., and M. Glaser. 1993. Distributions of proteins and lipids in the erythrocyte membrane. *Biochemistry.* 32:12591–12598.

Sandison, D. R., D. W. Piston, and W. W. Webb. 1994. Background rejection and optimization of signal to noise in confocal microscopy. *In* Three-Dimensional Confocal Microscopy: Volume Investigation of Biological Systems. J. K. Stevens, L. R. Mills, and J. E. Trogadis, editors. Academic Press, Inc. 29–45.

Sankaram, M. B., D. Marsh, L. M. Gierasch, and T. E. Thompson. 1994. Reorganization of lipid domain structure in membranes by a transmembrane peptide—an ESR spin label study on the effect of the *Escherichia Coli* outer membrane protein a signal peptide on the fluid lipid domain connectivity in binary mixtures of dimyristoyl phosphatidylcholine and distearoyl phosphatidylcholine. *Biophys. J.* 66:1959–1968.

Sankaram, M. B., D. Marsh, and T. E. Thompson. 1992. Determination of fluid and gel domain sizes in two-component, two-phase lipid bilayers. *Biophys. J.* 63:340–349.

Serafini, B., A. Cimini, M. Sette, and C. Aartori. 1993. P-31-NMR of liver peroxisome membranes from normal and clofibrate-treated rats. *Cell. Mol. Biol.* 39:479–489.

Sewell, W. F., and E. A. Mroz. 1993. Flavin adenine dinucleotide is a major endogenous fluorophore in the inner ear. *Hearing Res.* 70:131–138.

Singer, S. J. 1990. The structure and insertion of integral proteins in membranes. *Annu. Rev. Cell Biol.* 6:247–296.

Singer, S. J., and G. L. Nicolson. 1972. The fluid mosaic model of the structure of cell membrane. *Science.* 175:720–731.

So, P. T. C., T. French, W. M. Yu, K. M. Berland, C. Y. Dong, and E. Gratton. 1995. Time-resolved fluorescence microscopy using two-photon excitation. *Bioimaging.* (In press.)

Stossel, T. P. 1993. On the crawling of animal cells. *Science.* 260:1086–1094.

Suzuki, K., Y. Tanaka, Y. Nakajima, K. Hirano, K. Itoh, H. Miyata, T. Hayakawa, and K. Kinosita. 1995. Spatiotemporal relationships among

early events of fertilization in sea urchin eggs revealed by multiview microscopy. *Biophys. J.* 68:739–748.

Vigh, L., D. A. Los, I. Horvath, and N. Murata. 1993. The primary signal in the biological perception of temperature: Pd-catalyzed hydrogenation of membrane lipids stimulated the expression of the desA gene in *Synechocystis* PCC6803. *Proc. Natl. Acad. Sci. USA.* 90:9090–9094.

Wang, Y., and R. I. Hollingsworth. 1995. A solvent system for the high-resolution proton nuclear magnetic resonance spectroscopy of membrane lipids. *Anal. Biochem.* 225:242–251.

Wang, X. F., J. J. Lemasters, B. Herman, and S. C. Kuo. 1993. Multiple microscopic techniques for the measurement of plasma membrane lipid structure during hypoxia. *Opt. Eng.* 32:284–290.

Weber, G., and F. J. Farris. 1979. Synthesis and spectral properties of a hydrophobic fluorescence probe: 6-propionyl-2-(dimethylamino)naphthalene. *Biochemistry.* 18:3075–3078.

Wells, K. S., D. R. Sandison, J. H. Strickler, and W. W. Webb. 1989. Quantitative fluorescence imaging with laser scanning confocal microscopy. *In* Handbook of Biological Confocal Microscopy. J. Pawley, editor. IMR Press, Madison, WI. 23–34.

Williams, R. M., D. W. Piston, and W. W. Webb. 1994. Two-photon molecular excitation provides intrinsic 3-dimensional resolution for laser-based microscopy and microphotochemistry. *FASEB J.* 8:804–813.

Wolf, D. E., V. M. Maynard, C. A. McKinnon, and D. L. Melchior. 1990. Lipid domains in the ram sperm plasma membrane demonstrated by differential scanning calorimetry. *Proc. Natl. Acad. Sci. USA.* 87: 6893–3896.

Zhang, F., G. M. Lee, and K. Jacobson. 1993. Protein lateral mobility as a reflection of membrane microstructure. *Bioessays.* 15:579–588.